



**HAL**  
open science

## Analysis of InGaN surfaces after chemical treatments and atomic layer deposition of Al<sub>2</sub>O<sub>3</sub> for uLED applications

Corentin Le Maout, David Vaufrey, François Martin, Eugénie Martinez,  
Emmanuel Nolot, Stéphane Cadot, Etienne Gheeraert

► **To cite this version:**

Corentin Le Maout, David Vaufrey, François Martin, Eugénie Martinez, Emmanuel Nolot, et al.. Analysis of InGaN surfaces after chemical treatments and atomic layer deposition of Al<sub>2</sub>O<sub>3</sub> for uLED applications. Proceedings of SPIE, the International Society for Optical Engineering, 2020, 11280, pp.112801C. 10.1117/12.2544787 . cea-02941396v1

**HAL Id: cea-02941396**

**<https://cea.hal.science/cea-02941396v1>**

Submitted on 17 Sep 2020 (v1), last revised 25 Sep 2020 (v2)

**HAL** is a multi-disciplinary open access archive for the deposit and dissemination of scientific research documents, whether they are published or not. The documents may come from teaching and research institutions in France or abroad, or from public or private research centers.

L'archive ouverte pluridisciplinaire **HAL**, est destinée au dépôt et à la diffusion de documents scientifiques de niveau recherche, publiés ou non, émanant des établissements d'enseignement et de recherche français ou étrangers, des laboratoires publics ou privés.

# PROCEEDINGS OF SPIE

[SPIDigitalLibrary.org/conference-proceedings-of-spie](https://spiedigitallibrary.org/conference-proceedings-of-spie)

## Analysis of InGaN surfaces after chemical treatments and atomic layer deposition of Al<sub>2</sub>O<sub>3</sub> for $\mu$ LED applications

Le Maout, Corentin, Vaufrey, David, Martin, François, Martinez, Eugénie, Nolot, Emmanuel, et al.

Corentin Le Maout, David Vaufrey, François Martin, Eugénie Martinez, Emmanuel Nolot, Stéphane Cadot, Etienne Gheeraert, "Analysis of InGaN surfaces after chemical treatments and atomic layer deposition of Al<sub>2</sub>O<sub>3</sub> for  $\mu$ LED applications," Proc. SPIE 11280, Gallium Nitride Materials and Devices XV, 112801C (16 February 2020); doi: 10.1117/12.2544787

**SPIE.**

Event: SPIE OPTO, 2020, San Francisco, California, United States

# Analysis of InGaN surfaces after chemical treatments and atomic layer deposition of Al<sub>2</sub>O<sub>3</sub> for $\mu$ LED applications

Corentin Le Maoult<sup>a</sup>, David Vaufrey<sup>a</sup>, François Martin<sup>a</sup>, Eugénie Martinez<sup>a</sup>, Emmanuel Nolot<sup>a</sup>, Stéphane Cadot<sup>a</sup>, Etienne Gheeraert<sup>b</sup>

<sup>a</sup>Univ. Grenoble Alpes, CEA, LETI, F-38000 Grenoble, France; <sup>b</sup>Univ. Grenoble Alpes, CNRS, Grenoble INP\*, Institut Néel, 38000 Grenoble, France

## ABSTRACT

A deep understanding of semiconductors-dielectrics interface properties will provide guidelines to optimize efficient passivation solutions for InGaN/GaN based  $\mu$ LED. To this end, the quantum wells (QW) semiconductor is of tremendous interest since a lot of surface recombinations are likely to occur at LED active regions edges and are probably responsible for the low  $\mu$ LED efficiencies. Thus we discuss in this paper about X-ray photoemission (XPS) and wavelength dispersive X-ray fluorescence (WDXRF) characterizations of In<sub>0.1</sub>Ga<sub>0.9</sub>N surfaces after acid, basic or sulfur based chemical treatments followed or not by atomic layer deposition (ALD) of Al<sub>2</sub>O<sub>3</sub> thin films with TMA/H<sub>2</sub>O or TMA/O<sub>2</sub> plasma (plasma enhanced ALD) at 250°C.

Depending on chemical treatments, variations of indium related XPS peaks were observed, which did not seem to be significantly affected by deposition of Al<sub>2</sub>O<sub>3</sub> whatever the oxidizing precursor. The extreme surface concentration of indium was probably reduced, suggesting that some chemical pre-treatments for cleaning or passivation steps would have a direct impact on InGaN QW properties at LED edges.

After sulfur based chemical treatments, even if sulfur was hardly detected by XPS, complementary measurements by WDXRF and subsequent calibration of the sulfur signal supported evaluation of a low surface concentration of sulfur.

Changes of Al<sub>2</sub>O<sub>3</sub> related XPS peaks suggested that the various studied pre-treatments induced different nucleations of first ALD cycles. Then, a clear variation of InGaN surfaces hydrolysis depending on surface treatments was finally highlighted by WDXRF based counting measurements, opening the way to a better understanding of first Al<sub>2</sub>O<sub>3</sub> layers nucleation on InGaN.

**Keywords:** \* $\mu$ LED, InGaN passivation, XPS-WDXRF, Al<sub>2</sub>O<sub>3</sub>-ALD or PEALD, surface treatments\*

## 1. INTRODUCTION

III-V materials have allowed the development of very efficient blue planar light emitting diodes (LED) for display or lighting applications. Because of relatively new applications such as micro-displays, LED miniaturization is becoming an attractive challenge of recent years in optoelectronics. Especially since micro-sized GaN/InGaN LED ( $\mu$ LED) seem to offer very promising properties particularly adapted to this field.

Indeed, according to the literature,  $\mu$ LED would allow good viewing angles<sup>1</sup> and would handle higher current densities than macro-LED, presumably thanks to better current and thermal managements in devices. Consequently,  $\mu$ LED would be capable of reaching higher optical output power densities than macro-LED<sup>2-6</sup>. However, extraction efficiency would also have to be considered at this point (some optical modes are strongly geometry and dimensions dependent). Some discussions report also about GaN/InGaN strain constraint relaxations in  $\mu$ LED<sup>6-8</sup> comparatively to macro-LED. All these considerations being still under debate.

However, huge luminescence efficiency decreases have been observed for  $\mu$ LED, presumably attributed to etching related sidewalls defects states and size effects<sup>5,9,10</sup>. Besides optimizing etching processes to limit sidewalls defects generation, the development and the optimization of passivation post-processing steps seem to be mandatory at this point. Thus, it represents a key point of interest since efficient  $\mu$ LED sidewall passivation solutions would allow to significantly improve the current GaN/InGaN  $\mu$ LED technology.

Some research teams already presented LED passivation related solutions. During the first decade of the 2000s, first examples of LED efficiency improvements after deposition of SiN<sup>11</sup>, SiON<sup>12</sup> or even Al<sub>2</sub>O<sub>3</sub><sup>13</sup> layers could be found in literature. A better extraction was achieved using the thin dielectric layers as an optical index adaptation tool. Later, Yang

et al.<sup>14</sup> and Guo et al.<sup>15</sup> presented first detailed studies of Al<sub>2</sub>O<sub>3</sub> deposition effects on LED electrical properties. While they added a top SiO<sub>2</sub> layer mainly for extraction considerations, it was shown that ALD or PEALD of Al<sub>2</sub>O<sub>3</sub> from their Al<sub>2</sub>O<sub>3</sub>-SiO<sub>2</sub> stacks allowed LED electro-optical properties improvements thanks to surface states densities lowering. Another document also reports the passivation efficiency of SiO<sub>2</sub>-Si<sub>3</sub>N<sub>4</sub> stacks deposited by PECVD<sup>16</sup> despite the plasma deposition. Finally, Wong et al.<sup>17</sup> were the first to demonstrate an improved efficiency on  $\mu$ LED after ALD of SiO<sub>2</sub>, and highlighted the importance of using preferentially ALD method rather than PECVD. Very recently, for LED holes injections related problematics, Kim et al.<sup>18</sup> managed to control the bands bending of p-GaN surface after ALD of AlN-Al<sub>2</sub>O<sub>3</sub> stacks. A clear improvement of their LED efficiency was achieved thanks to a better p-GaN passivation coupled to an increased holes injection efficiency in the LED active region.

These first LED passivation-related works are often focused on extraction problematics and mostly concern macro-sized LED. Few of them treat exclusively of  $\mu$ LED passivation issues. In this context, detailed studies focusing separately on LED semiconductors surface properties after typical passivation steps will undoubtedly provide solid, complementary and helpful knowledge to go further in developing the best passivation solution for GaN/InGaN  $\mu$ LED. Due to their different compositions or doping natures, transport layers and active region semiconductors from LED structures cannot be handle similarly for passivation problematics. Indeed, LED stacks include several semiconductors such as negatively doped GaN (n-GaN), positively doped GaN (p-GaN), AlGaN as electron blocking layer (EBL) and InGaN for the active region's QW.

Whether being bulk or surfaces related, Shockley-Read-Hall (SRH) non-radiative phenomena rate directly depends on the nature and concentration of the defects in LED and on charges carriers concentrations<sup>19</sup>.

Bulk defects proportion in LED mainly depends on epitaxy quality. On the contrary, surfaces defects mainly originate from etching steps (besides being also the natural consequence of inevitable dangling bonds at the surface). For  $\mu$ LED, the high perimeter to surface ratio is responsible for an increased sensitivity to surface defects and thus to the SRH associated recombinations.

Numerical simulation results, displayed in figure 1, confirm that SRH recombinations mainly occur in LED stack layers with high hole and electron concentration overlapping. Consequently, SRH recombination rate is higher in quantum wells since obviously the LED bandgap engineering concentrates opposite sign carriers in InGaN layers to optimize the radiative recombinations. Due to electronic overflow and GaN p-doping difficulties, the p-doped transport layers present a relatively high minority charge carrier concentration comparatively to the n-GaN layers. Therefore, InGaN from the active region would have to be considered preferentially for passivation problematics. Then, the p-GaN and finally the n-GaN.

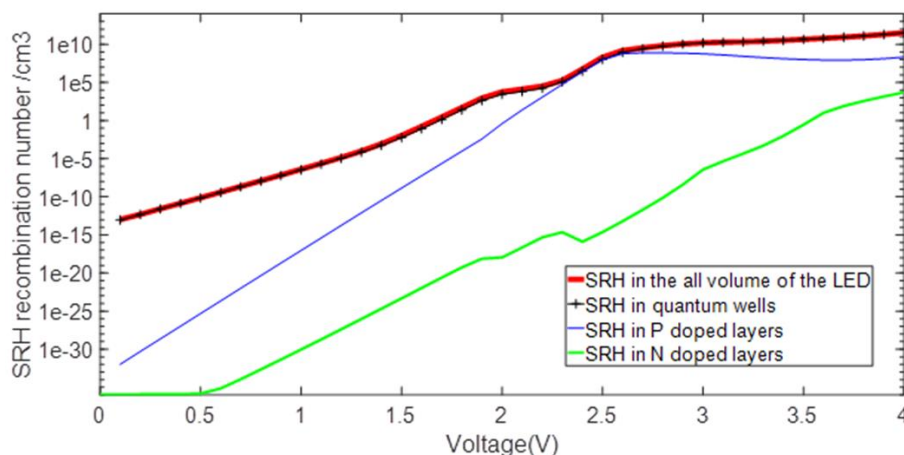


**Fig. 1.** SRH recombination number/cm<sup>3</sup> in various volumes of a GaN based LED modelled with ATLAS from Silvaco

Regarding dielectric materials, as previously mentioned, scientific publications underline the potential effectiveness of SiO<sub>2</sub> or Al<sub>2</sub>O<sub>3</sub> for LED sidewall passivation. Additionally, the passivating action of alumina over GaN surfaces is often reported for power transistor applications, especially when oxidizing reactant is tuning the bandgap value and leakage characteristics of alumina (ALD versus PEALD)<sup>20</sup>. Al<sub>2</sub>O<sub>3</sub> and SiO<sub>2</sub> have a large band gap ( $E_g \sim 7-9$ eV), large conduction and valence bands offsets (respectively  $\sim 2.1$ eV and  $\sim 2.5$ eV for Al<sub>2</sub>O<sub>3</sub>,  $\sim 3.6$ eV and  $\sim 2$ eV for SiO<sub>2</sub><sup>21</sup>) and an 1.8 (1.48 for SiO<sub>2</sub>) optical index (at 450nm), which could be valuable for internal reflection in LED ( $n_{\text{GaN}(450\text{ nm})} \sim 2.49$ ). The free Gibbs

energy of  $\text{Al}_2\text{O}_3$  formation reaction ( $-1582 \text{ kJ}\cdot\text{mol}^{-1}$ ) is also higher than  $\text{Ga}_2\text{O}_3$  value for example ( $-998 \text{ kJ}\cdot\text{mol}^{-1}$ )<sup>22</sup>. Finally, ALD  $\text{Al}_2\text{O}_3$  is a well-known deposition process and is also recognized as non surface-damaging method. Besides allowing a very precise thickness control, uniform and homogeneous nanometer-thick layers can be deposited with ALD on surfaces with low or high aspect ratio factors. For all these reasons, ALD alumina seems to be particularly suitable for LED sidewalls passivation problematics, provided  $\text{Al}_2\text{O}_3$  reactant would be chosen after evaluation of its oxidizing power over LED stack semiconductor's ( $\text{H}_2\text{O}$ ,  $\text{O}_3$ ,  $\text{O}_2$  plasma...).

This document deals with surfaces properties of InGa $_x$ N after standard surface chemical treatments such as HCl or  $\text{NH}_4\text{OH}$  before ALD of  $\text{Al}_2\text{O}_3$  using different oxidizing reactants. Effects of  $(\text{NH}_4)_2\text{S}$  surface treatments are also evaluated, since several scientific publications report the sulfur passivating action effectiveness over GaN surfaces, presumably strongly dependent on experimental conditions<sup>23</sup>. Indeed, InGa $_x$ N surface study allows us to investigate in the same time, gallium and indium evolution induced by surface treatment and/or ALD process. In particular, this study focus on indium and gallium oxidation and stoichiometry. Indeed, indium oxide is amphoteric, could act as a metal or as a semiconductor and consequently is expected to induce parasitic surface states. Equally, five polymorphs of gallium oxide are commonly identified and can be either insulators or conductors, depending on the growth conditions<sup>24,25</sup>. So, gallium oxide is also expected to induce parasitic surface states.

Furthermore, this study also focus on surface hydrolysis which promote dielectric nucleation such as ALD  $\text{Al}_2\text{O}_3$ . For this purpose, our investigations are based on X-ray photoelectron spectroscopy and high resolution wavelength dispersive X-ray fluorescence techniques, particularly adapted to surface qualitative or quantitative analysis.

## 2. EXPERIMENTAL

All experiments were performed on unpatterned and undoped samples with a 200nm  $\text{In}_x\text{Ga}_{1-x}\text{N}$  top layer ( $x \approx 10\%$ ) deposited on GaN buffer and sapphire substrates.

All samples were first cleaned using standard solvent solutions (acetone, ethanol then isopropyl alcohol). In the rest of the present document, samples at this stage will be referred as "as-received" samples. The HCl ( $\text{NH}_4\text{OH}$ ) treatments consisted in dipping samples in a mixture of 37% HCl (29%  $\text{NH}_4\text{OH}$ ) diluted 10 times in deionized (DI) water for 10 minutes at 300K. After treatments, samples were rinsed in DI water.

Sulfur chemical treatments were performed for 5 or 30 minutes in undiluted 20%  $(\text{NH}_4)_2\text{S}$  solutions at ambient temperature, after or not a first  $\text{NH}_4\text{OH}$  treatment. Different rinsing durations in DI water were implemented after the  $(\text{NH}_4)_2\text{S}$  treatments (as well as an IPA rinsing successively to a first DI water rinsing for one sample). Some reference samples were also exposed to sulfur using reaction at higher temperature.

Atomic layer depositions of  $\text{Al}_2\text{O}_3$  were all performed at 250°C using Oxford Fiji tool. The metallic precursor was trimethyl-aluminum (TMA). The oxidizing reactant was water ( $\text{H}_2\text{O}$ ) for thermal-based processes and oxygen radicals generated by the deposed plasma for the  $\text{O}_2$ -plasma processes.

Three-nanometers thick layers were deposited to allow the characterization of InGa $_x$ N/ $\text{Al}_2\text{O}_3$  interface by XPS measurements, given the limited sampling depth of XPS. Considering ALD equipment calibrations, it was equivalent to 30 cycles of ALD ( $\text{H}_2\text{O}$  first) and to 33 cycles of PEALD (TMA first). Sequences between surface treatments and  $\text{Al}_2\text{O}_3$  deposition were all completed in less than 5 minutes with an air break.

The thermal treatments were realized in a rapid thermal annealing furnace at 400°C during 15 minutes under dinitrogen atmosphere ( $\text{N}_2$ ), additionally to a 2 minutes long temperature rise and to 6 minutes of cooling.

XPS analyses were carried out with a spectrometer from Scienta Omicron equipped with a monochromated Al K $\alpha$  source ( $h\nu=1486.7\text{eV}$ ) and installed at the NanoCharacterization PlatForm (PFNC) of Minatec (Grenoble, France). Experiments were performed under ultra-high vacuum ( $P=10^{-9}$  mbar). Photoelectrons were collected by a hemispherical analyzer at pass energy of 15eV leading to an overall energy resolution of 350meV. All XPS analyses were done with a 80° angle between samples surfaces and analyzer; 1eV of flood-gun was applied to prevent surface from overcharging because of atoms ionization.

The C1s, Ga3d, In3d, N1s and O1s photoemission lines were collected for all samples. Al2p and/or S2p and S2s lines were added respectively after  $\text{Al}_2\text{O}_3$  deposition and/or after sulfured surface treatments. All XPS spectra were energy corrected referring to the C1s line fixed at 284.8eV. Quantitative analyses were performed after XPS spectra decompositions with the software CASAXPS, using Voigt functions and after adapted background subtraction. All energy lines subject to spin-orbit energy states splitting were decomposed using constrained doublets components.

The C1s line was decomposed using three components representative of C-C, C-O or O-C=O bonding. Then, two contributions representative of GaN(-In) and InN(-Ga) species with two additional oxide components ( $Ga_xO_y$  and  $In_xO_y$ , respectively constrained at +0.8eV and +0.6eV) were added respectively for Ga3d and In4d lines decompositions. Finally, two components representative of N2s and O2s lines were added near the Ga3d spectra respectively at lower and higher energies (O2s for  $Al_2O_3$  capped surfaces only). The In3d doublet was decomposed in two main components similarly to the In4d doublet ( $In_xO_y$  and InN(-Ga)). Due to the strong interference of the N1s line with gallium Auger peaks when the Al K $\alpha$  XPS source is used, nitrogen is not discussed in this paper. The O1s peak has been decomposed using three components accounting for oxygen-metalloid bonding (O-Ga and O-In), O-C/O-H and O=C bonding, respectively in the increased binding energy order. With the  $Al_2O_3$  dielectric layer, the peak composition was evolving in two main contributions representative of  $Al_2O_3$  and of Al-OH related species<sup>26</sup> at higher energy (constrained to +1.4eV from the  $Al_2O_3$  component). Note that O-C bonding from hydrocarbon contamination can also contribute to the higher energy peak. The Al2p peak was decomposed using a main contribution representative of  $Al_2O_3$  signal. In some cases, another component could be possibly added at high energy with respect to the  $Al_2O_3$  peak, representative of Al(OH)<sub>3</sub> species<sup>27</sup>. The S2p line is strongly interfering with the Ga3s line and with the associated gallium oxide. Consequently, the main S2p<sub>3/2</sub> peak of the S2p doublet was constrained between 163,5eV and 164,5eV. When visible, the S2s line was decomposed in two main components, possibly representative of Ga-S or In-S related species.

The growth of ALD  $Al_2O_3$  depends on the presence of -OH species at samples surfaces. Therefore, the counting of aluminum atoms chemisorbed after a first TMA exposition can be representative of the initial OH surface concentration (or surface hydrolysis). This quantitative analysis was performed using WDXRF measurements on InGaN surfaces after 1, 3 or 6 ALD cycles (TMA 1<sup>st</sup>) and depending on surface treatments (HCl,  $NH_4OH$  or  $(NH_4)_2S$  pre-treatments).

Complementary surface quantitative analysis of sulfur treated samples was performed by WDXRF measurements. A 3nm ZnS reference is used for sulfur calibration to estimate deconvolution validity, since a 4<sup>th</sup> diffraction order of the Ga K $\alpha$  line was interfering with the studied S K $\alpha$  line. Some "as-received" reference samples treated by the higher sulfidation temperature process are used for XPS calibration of  $(NH_4)_2S$  treated samples as well.

In-line wavelength-dispersive X-ray fluorescence (WDXRF) experiments were carried out in the primary-vacuum chamber of Rigaku AZX400 tool. The samples were irradiated with the polychromatic radiation of a Rhodium tube operated at 30 kV and 100 mA. We selected these conditions in order to enhance the intensity of Rhodium L lines (L $\alpha$  at 2.697 keV), thereby increasing the sensitivity to sulfur (using S-K $\alpha$  line) and aluminum (with Al-K $\alpha$  line). We used Ge (111) crystal (resp. a PET crystal) mounted on a high-resolution goniometer to select the wavelengths related to S-K $\alpha$  (resp. Al-K $\alpha$  line). Then, the X-ray fluorescence intensities were recorded with a gas flow type proportional counter. We used fundamental parameters approach<sup>28</sup> to quantify the deposited mass of aluminum. The sensitivity factor of the WDXRF tool was deduced from the measurement of a pure aluminum target.

### 3. XPS AND WDXRF STUDY OF INGAN SURFACE TREATMENT

#### 3.1 Comparison of InGaN surfaces after HCl or $NH_4OH$ chemical treatments

An important variation of the In4d peak intensities near the Ga3d spectra (fig. 2a) is evidenced after the HCl or  $NH_4OH$  chemical treatments, and especially after HCl.

The quantitative analysis summarized in figure 3 reports a total indium relative atomic concentration estimated at approximatively 13 at.% for as-received samples decreasing until 12 at.% and 5 at.%, respectively after  $NH_4OH$  and HCl treatments. Similar trends are observed whether analysis is done using In3d or In4d photoemission lines (fig. 3). Oxygen levels seem to decrease from 10 at.% for the as-received sample to about 8 at.% and 5 at.% with  $NH_4OH$  and HCl treatments respectively (fig. 3).

In comparison, gallium atomic concentration and oxide level do not significantly change according to the proposed decompositions and to the resulting quantitative analysis detailed in figure 3 (the gallium content is however increased for HCl treated sample, consequently to indium depletion). The same ascertainment can be done for oxidized carbon contributions, even if a slight decrease can be noted for HCl treated sample.

Consequently, indium and oxygen intensities attenuations could be partially induced by the decrease of indium oxidation level. This is consistent with the In3d shape evolutions. Indeed, as illustrated in figure 2b, indium is initially quite oxidized since we have relatively symmetrical and broad peaks, while a much thinner and asymmetrical contribution

seems to dominate at lower energy after both chemical treatments. Moreover, the low energy O1s contribution generally representative of oxygen-metalloids bonding is attenuated after both chemical treatments but especially after HCl (fig. 2c).

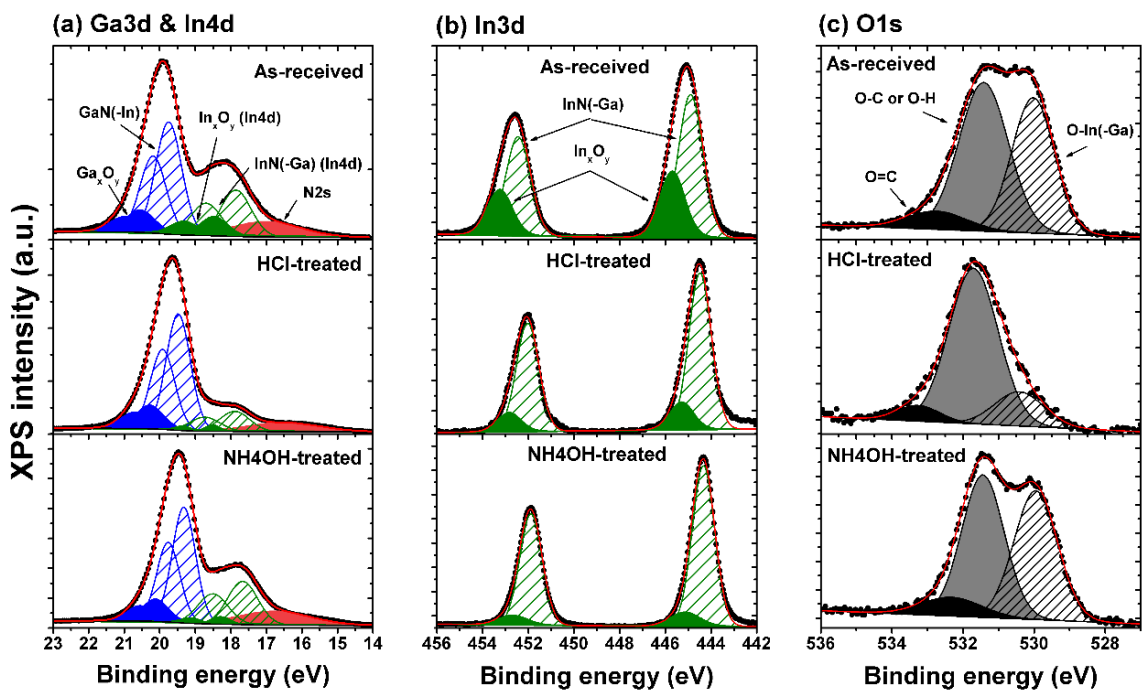


Fig. 2. Ga3d & In4d (a), In3d (b), O1s (c) spectra after HCl or NH4OH

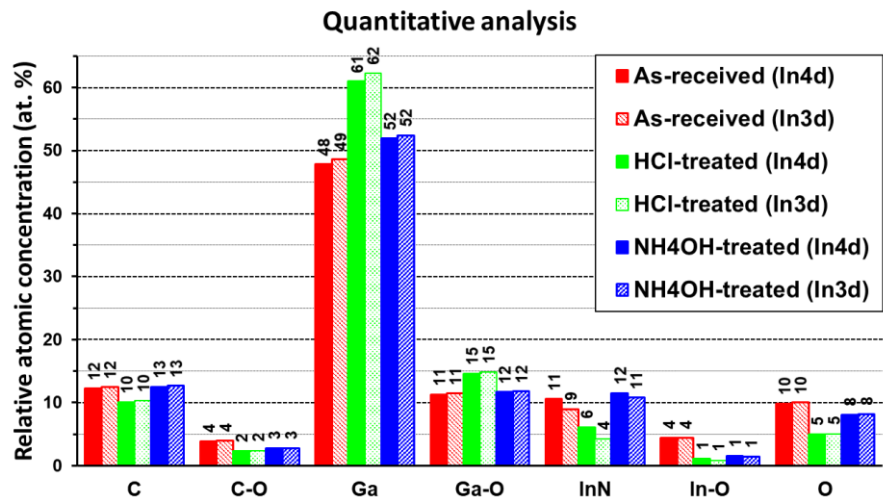


Fig. 3. Relative atomic concentrations estimated from XPS quantitative analysis of samples after HCl or NH4OH treatments, using In3d or In4d lines

Considering that the indium level decrease is larger than oxygen level variations, it appears also that besides indium oxidation decrease, indium preferential etching or desorption at the surface is likely to occur significantly during a HCl cleaning, whatever it would be oxidized or not.

Besides the oxygen-metalloids component variations of the O1s peak, there is no clear differences at the O1s higher energies between NH<sub>4</sub>OH or HCl treated samples (fig. 2c). Since the O1s composition at the higher energy range could be associated to O-C or O-H species, we could not conclude about surface hydrolysis exclusively based on XPS analysis.

Similarly, a clear In-OH related component could not be identified at In3d peak's high energies from any samples (fig. 2b), as shown before on some III-V compounds<sup>29</sup>. Provided InGaN alloys could behave in the same way, these results would not suggest indium to significantly bond with OH-related species after NH<sub>4</sub>OH treatment considering XPS analysis scope.

### 3.2 Evaluation of sulfur based chemical treatments effectiveness on InGaN surfaces

The same experiments is performed after implementing (NH<sub>4</sub>)<sub>2</sub>S treatments. As for HCl, a strong decrease of In4d peak near the Ga3d spectra is also induced by (NH<sub>4</sub>)<sub>2</sub>S chemical treatments (as shown in figure 4a). The decrease is stronger than observed previously with HCl and seems to be slightly dependent on treatment duration or pre-treatment. Indeed, the quantitative analysis of figure 4c reports a total indium content reduced to 3 at.% after the 5' (NH<sub>4</sub>)<sub>2</sub>S treatment and hardly reaching 2 at.% after 30' (NH<sub>4</sub>)<sub>2</sub>S treatment (with or without NH<sub>4</sub>OH pre-treatment). Again, similar trends are obtained whatever the indium photoemission line used for quantification. Therefore, sulfur based chemical treatments such as (NH<sub>4</sub>)<sub>2</sub>S would also induce a preferential etching of indium as observed previously with HCl solutions.

Moreover, the sulfur is expected to passivate the surfaces, preventing InGaN atoms from re-oxidizing after treatments. Indeed, a decrease of the oxygen content (fig. 4c) associated with a strong reduction of the low energy oxygen-metalloid related components (fig. 4b) is also observed. With the exception of samples treated with (NH<sub>4</sub>)<sub>2</sub>S only 5', the NH<sub>4</sub>OH pre-treatment does not seem to induce further oxygen level decrease. Typically, while the total oxygen content is about 10 at.% for the as-received sample, the latter decreases around 7-8 at.% after 5' treatment and hardly reaches 5-6 at.% after longer treatments.

Considering the ratios of figure 4d, the oxygen decrease is probably mainly attributed to the decrease of indium and carbon oxidized contributions, the gallium oxidation state being rather stable.

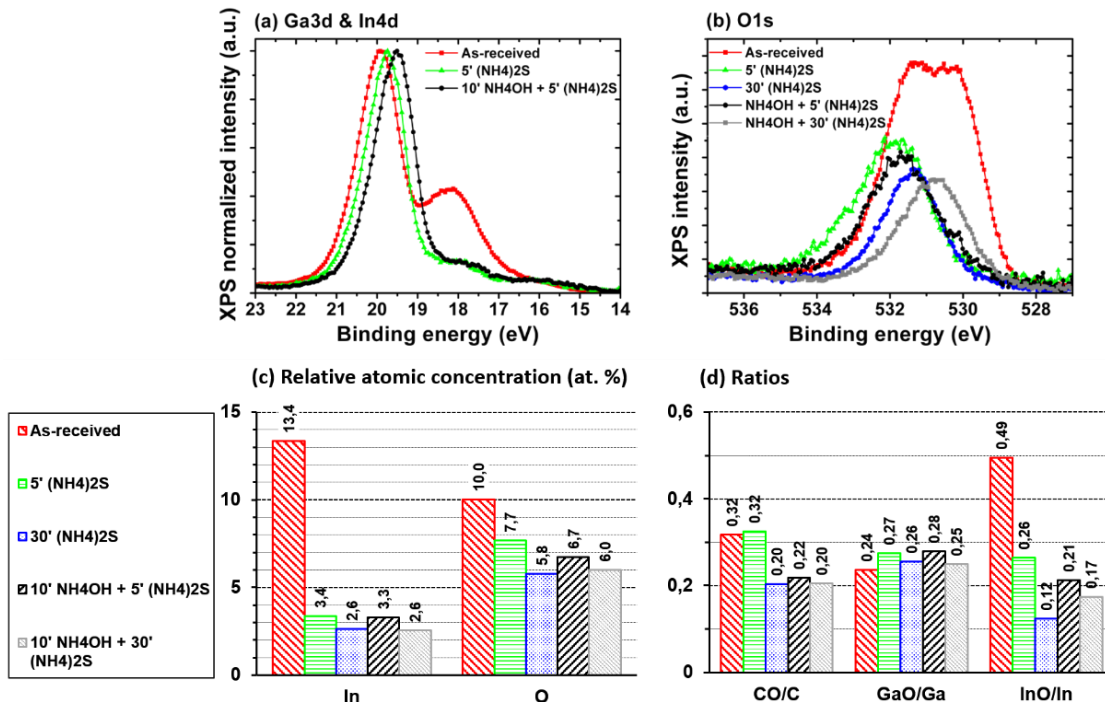


**Fig. 4.** (a) Superposition of Ga3d normalized XPS spectra of as-received, 5' (NH<sub>4</sub>)<sub>2</sub>S treated and NH<sub>4</sub>OH + 5' (NH<sub>4</sub>)<sub>2</sub>S treated samples (b) Superposition of O1s XPS spectra of the same samples and of 30' (NH<sub>4</sub>)<sub>2</sub>S treated and NH<sub>4</sub>OH + 30' (NH<sub>4</sub>)<sub>2</sub>S treated samples (c) Indium and oxygen In3d-based stoichiometric analysis (d) Oxidized/unoxidized components ratio

Sulfur is however hardly detected since no clear S2s or S2p contributions could be observed on these samples. As shown in figure 5a, a slightly broader spectrum would be obtained after (NH<sub>4</sub>)<sub>2</sub>S-treatment, if the sample is not rinsed at all. That could suggest the apparition of a small S2p doublet. However, due to the interference with Ga3s components (presumably with the oxide component) the very low intensity S2p doublet identification is quite speculative. Especially

in comparison to the clear S2p and S2s contributions observed on XPS spectra from the sulfur reference sample (fig. 5a & 5b). Therefore, considering the oxygen lowering, sulfur might be adsorbed at InGaN surface after (NH<sub>4</sub>)<sub>2</sub>S treatments but presumably in low proportion and in a state probably quite sensitive to process conditions such as rinsing and to environment. Indeed, several scientific publications highlight the impact of rinsing which tends to remove adsorbed sulfur on GaN surfaces<sup>23</sup>.

Then, the two distinct components that seems to appear on the S2s line from the sulfur reference sample (fig. 5b) might be representative of In-S or Ga-S bonds. Thus, the gallium or indium oxidized components previously estimated from our decompositions could actually integrate a X-S contribution (X being for Ga or In), as already reported in literature<sup>30</sup>. However, further investigations must be conducted in order to really conclude about sulfur bonds nature at InGaN surfaces.

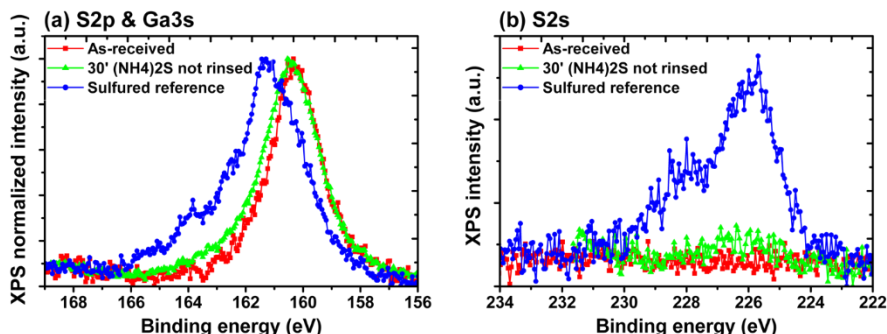


**Fig. 5.** (a) Superposition of S2p-Ga3s normalized XPS spectra of as-received, 30' (NH<sub>4</sub>)<sub>2</sub>S-treated and sulfur reference samples (b) Superposition of S2s spectra of the same samples

### 3.3 WDXRF measurements

The complementary WDXRF results from 30' (NH<sub>4</sub>)<sub>2</sub>S treated samples seem to reveal relatively similar doses of adsorbed sulfur atoms whether the samples were DI water or IPA rinsed (fig. 6). These results are comforted after calibration of the sulfur WDXRF peak position at 110.8° angle using the ZnS reference (fig. 6b & 6c). Indeed, the sulfur component is interfering with the Ga Kα 4<sup>th</sup> diffraction order. Based on those measurements, we would evaluate the sulfur dose after these treatments at 5-20 ng/cm<sup>2</sup>, which could be equivalent to a ~1-4.10<sup>14</sup> at.cm<sup>-2</sup> atomic surface density. Therefore, the sulfur proportion on the surface would not be negligible in comparison with the InGaN atomic surface density presumably around ~10<sup>15</sup> at.cm<sup>-2</sup>.

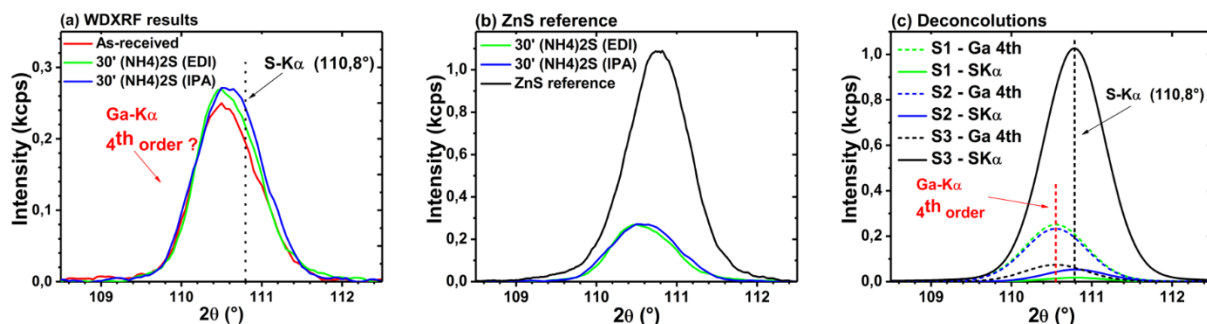


**Fig. 6.** (a) S Kα WDXRF measurements spectra of as-received sample and of 30' (NH<sub>4</sub>)<sub>2</sub>S treated samples with EDI or IPA rinsing (b) comparison with the spectrum obtained from a ZnS/InGaN reference (c) spectra deconvolution between the Ga Kα 4<sup>th</sup> diffraction order and the S Kα line (S1: 30' (NH<sub>4</sub>)<sub>2</sub>S treated with EDI rinsing; S2: 30' (NH<sub>4</sub>)<sub>2</sub>S treated with IPA rinsing; S3: ZnS reference)

Then, WDXRF-based counting measurements after the first TMA cycles were performed in order to indirectly evaluate the surface proportion of OH related species by TMA grafting. These results display a higher aluminum intensity after a NH<sub>4</sub>OH pre-treatment comparatively to untreated InGaN surfaces whatever the ALD cycle number (as displayed in figure 7a). The aluminum atomic surface density after 1 ALD TMA/H<sub>2</sub>O cycle is estimated to be about 4.2.10<sup>14</sup> at. cm<sup>-2</sup>

without treatment while being 50% higher ( $6,3 \cdot 10^{14} \text{ at. cm}^{-2}$ ) using  $\text{NH}_4\text{OH}$  treatment (fig. 7b). On the contrary, the aluminum dose is always lower in the case of  $\text{HCl}$  treated surfaces (typically, 15-20% lower than for the as-received surface). Therefore, that could be representative of an improved hydroxylation of the  $\text{InGaN}$  surface after the  $\text{NH}_4\text{OH}$  treatment.

While the curves slopes seem relatively similar for as-received and  $\text{NH}_4\text{OH}$  treated samples, the growth rate seems decreased in case of  $\text{HCl}$  and  $(\text{NH}_4)_2\text{S}$  treated surfaces (fig. 7b). This observation suggests that the growth regime of alumina in the first ALD cycles is affected by the initial surface treatment by a mechanism still under investigations.

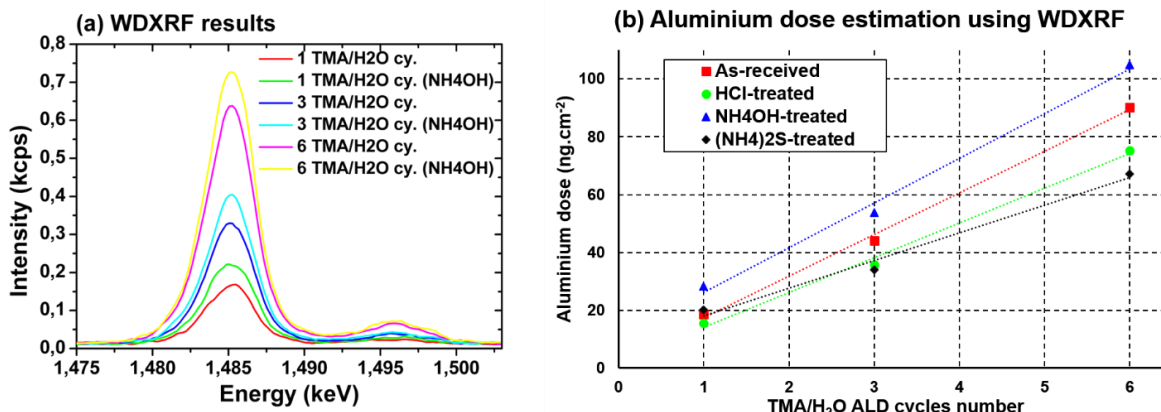


**Fig. 7.** (a) WDXRF Al intensities for as-received and  $\text{NH}_4\text{OH}$ -treated surfaces (b) WDXRF quantification estimation of the aluminum dose on the surfaces after 1, 3 or 6  $\text{TMA}(\text{H}_2\text{O})$  ALD cycles without surface treatment (as-received), with  $\text{HCl}$ ,  $\text{NH}_4\text{OH}$  or  $(\text{NH}_4)_2\text{S}$  surface treatment

Finally, to summarize the results obtained in this section, the most relevant features are the following:

- $\text{HCl}$  and  $(\text{NH}_4)_2\text{S}$  chemical treatments seem to induce a strong preferential etching of indium at the surface and therefore, an  $\text{InGaN}$  surface band gap increase. Considering LED structures and provided  $\text{InGaN}$  would behave the same way at LED sidewall, a larger gap could act as a potential barrier for charge carriers.
- $\text{NH}_4\text{OH}$  treatments promote hydrolysis of  $\text{InGaN}$  surfaces and probably a better nucleation of  $\text{Al}_2\text{O}_3$  thin layer during first cycles of ALD, opening presumably the way to a very good coverage of  $\text{InGaN}$  surface.
- $(\text{NH}_4)_2\text{S}$ -based chemical treatments are shown to induce oxygen level lowering of the  $\text{InGaN}$  surfaces. While XPS seems to be only relevant to evaluate the sulfidation effectiveness after higher temperature processes, WDXRF allows the evaluation of sulfur adsorption on  $\text{InGaN}$  surfaces after  $(\text{NH}_4)_2\text{S}$  treatments at ambient temperature.

#### 4. XPS STUDY OF THE ALD- $\text{Al}_2\text{O}_3$ /INGAN INTERFACE

In this part, the interfacial properties of  $\text{InGaN-Al}_2\text{O}_3$  depending on  $\text{Al}_2\text{O}_3$  deposition conditions or annealing will be discussed. The structural properties of the  $\text{Al}_2\text{O}_3$  layer depending on process condition will be evaluated as well.

When the surface is  $\text{Al}_2\text{O}_3$  capped, the  $\text{O}2s$  energy line interferes with the  $\text{Ga}3d$  spectra as illustrated in the figure 8a. Moreover, due to the lower kinetic energy of electrons and thus a higher attenuation, a strong XPS intensity decrease of the  $\text{In}3d$  line is also induced and tends to reduce the associated analysis precision. Since the  $\text{O}1s$  line is strongly dominated by  $\text{Al}_2\text{O}_3$  signal (as shown in figures 10a and 10b), the gallium and indium oxides identification has therefore been done after careful correlation of the different XPS spectra variations.

##### 4.1 Effect of reactant: ALD versus PEALD

The ALD of  $\text{Al}_2\text{O}_3$  with  $\text{H}_2\text{O}$  reactant (weak oxidizer) does not seem to induce a strong modification of the  $\text{InGaN}$  surface. We still observe an indium depletion since the  $\text{In}4d$  intensity decreases as observed previously on the  $\text{HCl}$  or  $\text{NH}_4\text{OH}$  treated surfaces only (top of figure 8a and figure 8b). On the contrary, during the PEALD of  $\text{Al}_2\text{O}_3$  (strong oxidizer), the  $\text{NH}_4\text{OH}$  treated surfaces have changed compared to  $\text{HCl}$  ones since the  $\text{In}4d$  component level is no longer distinguished from the PEALD reference (as illustrated by figures 8a, bottom, and 8b).

Then, if indium is assumed as being the main species sensitive to plasma induced oxidation, the indium depleted surfaces after HCl treatment would indeed remain in a quite stable state of oxidation whether ALD or PEALD process. On the contrary, the higher indium proportion from NH<sub>4</sub>OH treated surfaces is expected to be more likely oxidized by the plasma species.

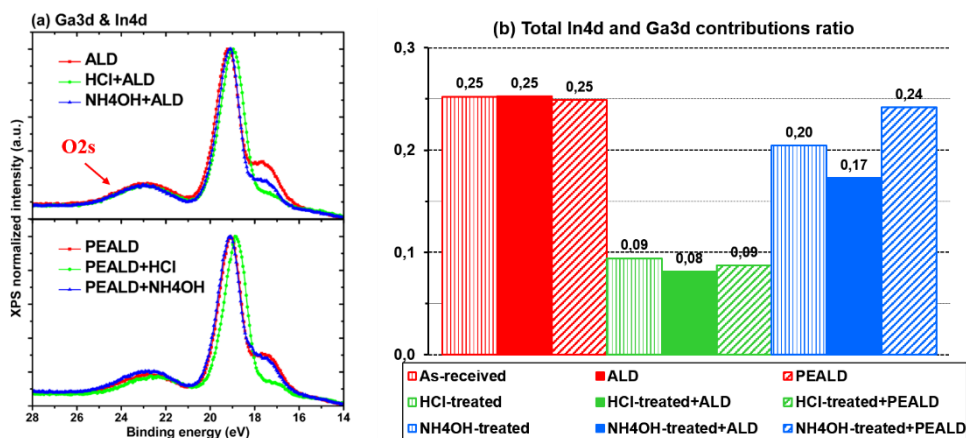


Fig. 8. (a) Superposition of normalized Ga3d-In4d spectra for ALD and PEALD samples without, with HCl or with NH<sub>4</sub>OH surface treatment (b) In4d/Ga3d ratios for the same samples in comparison with Al<sub>2</sub>O<sub>3</sub> free surfaces

## 4.2 ALD of Al<sub>2</sub>O<sub>3</sub> on sulfur passivation

If a 30' (NH<sub>4</sub>)<sub>2</sub>S surface treatment with or without a first NH<sub>4</sub>OH treatment is done before ALD, the quantitative analysis seems to report (figure 9b) similar results than observed previously without the alumina layer. As an example, a similar decrease scale of the indium proportion is observed (~75%). However, a slight increase of the O-Al related component from O1s line could be noted for the sample with the double surface treatment, probably related to the increased surface hydrolysis allowed by the first NH<sub>4</sub>OH treatment.

Thus, the ALD does not seem to induce strong modifications of the initial state of (NH<sub>4</sub>)<sub>2</sub>S-treated surfaces. However, these results do not provide quantitative information concerning sulfur proportion after Al<sub>2</sub>O<sub>3</sub> ALD deposition. Considering sulfur was assumed to be adsorbed on InGaN before deposition, further investigations would determine how sulfur bonds will evolve after ALD of Al<sub>2</sub>O<sub>3</sub> and especially if binding state differences with stronger oxidizing process such as PEALD would be visible.

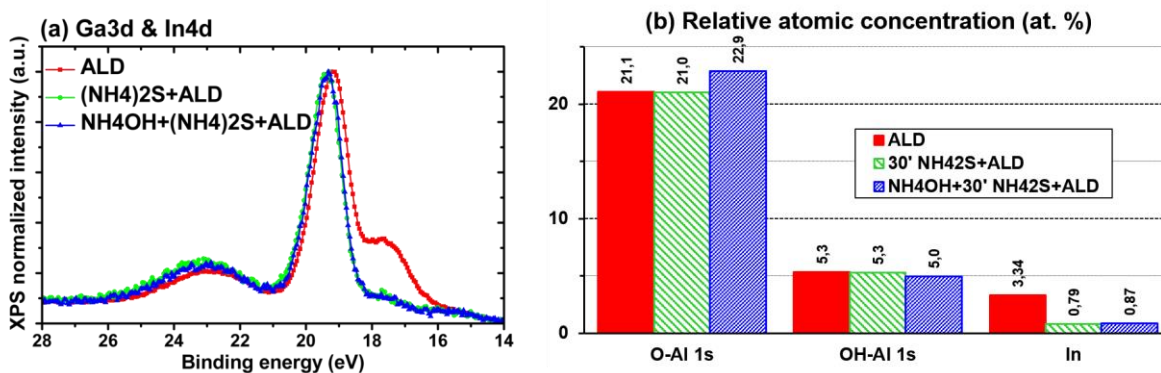
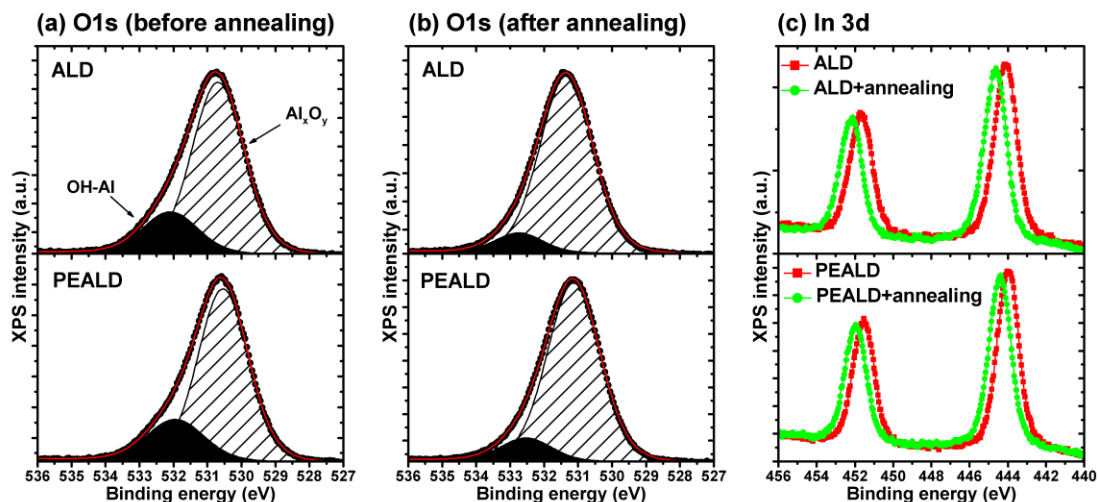


Fig. 9. (a) Superposition of Ga3d & In4d normalized XPS spectra of ALD-Al<sub>2</sub>O<sub>3</sub> samples without, with a 30' (NH<sub>4</sub>)<sub>2</sub>S or with a NH<sub>4</sub>OH+ 30' (NH<sub>4</sub>)<sub>2</sub>S surface treatment (b) Proportion of O1s components and total indium contribution using In4d line

### 4.3 Thermal annealing

The thermal annealing influence on the  $\text{Al}_2\text{O}_3/\text{InGaN}$  interface and  $\text{Al}_2\text{O}_3$  structural properties will now be discussed. Several studies on silicon report the release of hydrogenated species from the  $\text{Al}_2\text{O}_3$  layer, especially hydroxyls, after  $400^\circ\text{C}$  annealing. This effect has been qualitatively documented on silicon<sup>31</sup> but similar data does not exist for InGaN surfaces at equivalent annealing temperature.



**Fig. 10.** O1s XPS spectra measured for ALD- $\text{Al}_2\text{O}_3/\text{InGaN}$  and PEALD- $\text{Al}_2\text{O}_3/\text{InGaN}$  samples before (a) and after (b)  $400^\circ\text{C}$  thermal annealing (c) superposition of In3d XPS spectra from the same samples

After a  $400^\circ\text{C}$  thermal annealing, the O1s spectra reported in the figure 10 would suggest the OH related component to be decreased for both ALD and PEALD samples. Moreover, the quantitative analysis (fig. 11b) displays a significant decrease of Al-OH/ $\text{Al}_x\text{O}_y$  ratio from O1s line. Therefore, thanks to OH diffusion previously discussed and to thermally activated reactions, aluminum is probably reacting with oxygen to form preferentially  $\text{Al}_x\text{O}_y$  from  $\text{Al}(\text{OH})_x$  related species.

In the same way, the quantitative analysis of figure 11a seems to report a significant increase of the indium oxidation, as supported by In3d spectra evolution after annealing (fig. 10c). On the contrary, the gallium oxidized and GaN(-In) components ratio is comparatively much less affected (fig. 11b), which is coherent with the results presented in the first part. Therefore, these results would effectively confirm indium as the main element of the alloy sensitive to oxidizing species, associated in that case with hydroxyls released during the annealing.

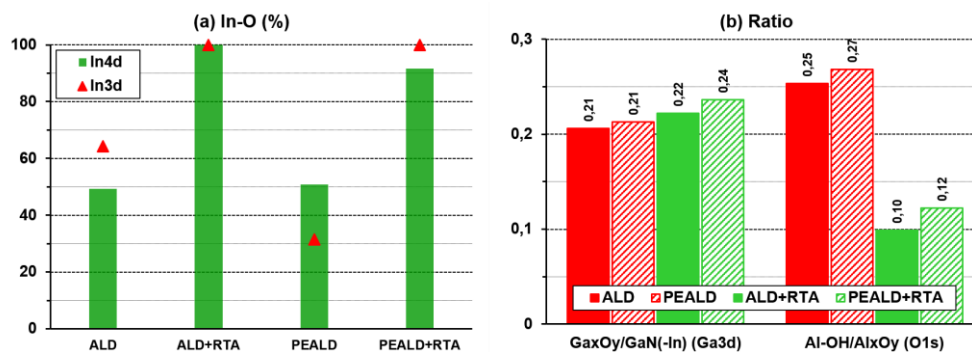


**Fig. 11.** (a) Estimation of In-O species proportion from indium related peak based on In4d and In3d quantitative analysis for annealed ALD and PEALD samples (b)  $\text{Ga}_x\text{O}_y/\text{GaN}(-\text{In})$  & Al-OH/ $\text{Al}_x\text{O}_y$  ratio for the same samples (respectively from Ga3d and O1s lines)

## 5. CONCLUSION

In this paper, a detailed study of LED QW semiconductor surface properties is reported after various passivation process steps. The XPS analysis suggested indium of InGaN compound to be preferentially etched by several surface treatments such as HCl or  $(\text{NH}_4)_2\text{S}$ . Moreover, indium appeared to be probably quite sensitive to oxidation while the oxidation state of gallium seemed globally quite stable through the studied surface treatments, annealing or plasma-based processes.

The sulfidation effect of  $(\text{NH}_4)_2\text{S}$  based chemical treatments at ambient temperature provided sulfur surface proportion below XPS sensitivity. However, thanks to the high resolution of WDXRF, we can estimate for the first time adsorbed sulfur in the range of  $10^{14}$  at.cm<sup>-2</sup>, and presumably bonded with gallium or indium by substitution of oxygen.

Moreover, WDXRF measurements highlighted the significance of the chemical pre-treatment or cleaning step before the deposition of a passivating dielectric such as  $\text{Al}_2\text{O}_3$  by ALD. Indeed, contrary to HCl or  $(\text{NH}_4)_2\text{S}$ ,  $\text{NH}_4\text{OH}$  was shown to promote the nucleation of an alumina layer during the first few ALD cycles, presumably thanks to a higher surface hydrolysis. Wettability experiments depending on surface treatments will certainly allow to support the previous assumption.

Complementary WDXRF investigations of  $\text{Al}_2\text{O}_3$  deposition on sulfur treated surfaces would now be of tremendous interest, especially in order to evaluate sulfur bonds stability depending on the oxidizing nature of deposition processes.

Additionally, electrical characterization such as C-V or DL(O)TS are required to correlate these qualitative observations with electrically active interface defects, especially after sulfidation related processes. The transposition of all these considerations to  $\mu\text{LED}$  sidewalls represents the next challenging step.

## ACKNOWLEDGEMENTS

This work has been performed with the help of the “Plateforme Technologique Amont” de Grenoble, with the financial support of CNRS Renatech network.

Facilities of the NanoCharacterization PlatForm (PFNC) used in this work are supported by the “Recherches Technologiques de Base” Program of the French Ministry of Research.

The authors acknowledge funding from the CleanSky-H2020 HILICO European project (under H2020-EU.3.4.5.6. - ITD Systems, Project ID: 755497).

## REFERENCES

- [1] Jiang, H. X., Jin, S. X., Li, J., Shakya, J. and Lin, J. Y., “III-nitride blue microdisplays,” *Appl. Phys. Lett.* **78**(9), 1303–1305 (2001).
- [2] Jin, S. X., Li, J., Li, J. Z., Lin, J. Y. and Jiang, H. X., “GaN microdisk light emitting diodes,” *Appl. Phys. Lett.* **76**(5), 631–633 (2000).
- [3] Jeon, C. W., Choi, H. W. and Dawson, M. D., “Fabrication of matrix-addressable InGaN-based microdisplays of high array density,” *IEEE Photonics Technology Letters* **15**(11), 1516–1518 (2003).
- [4] Gong, Z., Jin, S., Chen, Y., McKendry, J., Massoubre, D., Watson, I. M., Gu, E. and Dawson, M. D., “Size-dependent light output, spectral shift, and self-heating of 400 nm InGaN light-emitting diodes,” *Journal of Applied Physics* **107**(1), 013103 (2010).
- [5] Tian, P., McKendry, J. J. D., Gong, Z., Guilhabert, B., Watson, I. M., Gu, E., Chen, Z., Zhang, G. and Dawson, M. D., “Size-dependent efficiency and efficiency droop of blue InGaN micro-light emitting diodes,” *Appl. Phys. Lett.* **101**(23), 231110 (2012).
- [6] Dai, L., Zhang, B., Lin, J. Y. and Jiang, H. X., “Comparison of optical transitions in InGaN quantum well structures and microdisks,” *Journal of Applied Physics* **89**(9), 4951–4954 (2001).
- [7] Choi, H. W., Jeon, C. W., Dawson, M. D., Edwards, P. R., Martin, R. W. and Tripathy, S., “Mechanism of enhanced light output efficiency in InGaN-based microlight emitting diodes,” *Journal of Applied Physics* **93**(10), 5978–5982 (2003).

- [8] Tao, Y. B., Wang, S. Y., Chen, Z. Z., Gong, Z., Xie, E. Y., Chen, Y. J., Zhang, Y. F., McKendry, J., Massoubre, D., Gu, E. D., Rae, B. R., Henderson, R. K. and Zhang, G. Y., "Size effect on efficiency droop of blue light emitting diode," *physica status solidi c* **9**(3–4), 616–619 (2012).
- [9] Jin, S. X., Shakya, J., Lin, J. Y. and Jiang, H. X., "Size dependence of III-nitride microdisk light-emitting diode characteristics," *Appl. Phys. Lett.* **78**(22), 3532–3534 (2001).
- [10] Olivier, F., Daami, A., Licitra, C. and Templier, F., "Shockley-Read-Hall and Auger non-radiative recombination in GaN based LEDs: A size effect study," *Appl. Phys. Lett.* **111**(2), 022104 (2017).
- [11] Chang, K. M., Lang, C. C. and Cheng, C. C., "The Silicon Nitride Film Formed by ECR-CVD for GaN-Based LED Passivation," *physica status solidi (a)* **188**(1), 175–178 (2001).
- [12] Da, X., Guo, X., Dong, L., Song, Y., Ai, W. and Shen, G., "The silicon oxynitride layer deposited at low temperature for high-brightness GaN-based light-emitting diodes," *Solid-State Electronics* **50**(3), 508–510 (2006).
- [13] So, S.-J. and Park, C.-B., "Improvement of brightness with Al<sub>2</sub>O<sub>3</sub> passivation layers on the surface of InGaN/GaN-based light-emitting diode chips," *Thin Solid Films* **516**(8), 2031–2034 (2008).
- [14] Yang, C.-M., Kim, D.-S., Park, Y. S., Lee, J.-H., Lee, Y. S. and Lee, J.-H., "Enhancement in Light Extraction Efficiency of GaN-Based Light-Emitting Diodes Using Double Dielectric Surface Passivation" (2012).
- [15] Guo, H., Zhang, X., Chen, H., Liu, H., Zhang, P., Liao, Q., Hu, S., Chang, H., Sun, B., Wang, S. and Cui, Y., "High-Performance GaN-Based Light-Emitting Diodes on Patterned Sapphire Substrate with a Novel Patterned SiO<sub>2</sub>/Al<sub>2</sub>O<sub>3</sub> Passivation Layer," *Appl. Phys. Express* **6**(7), 072103 (2013).
- [16] Sheremet, V., Genç, M., Gheshlaghi, N., Elçi, M., Sheremet, N., Aydınli, A., Altuntaş, I., Ding, K., Avrutin, V., Özgür, ü. and Morkoç, H., "Two-step passivation for enhanced InGaN/GaN light emitting diodes with step graded electron injectors," *Superlattices and Microstructures* **113**, 623–634 (2018).
- [17] Wong, M. S., Hwang, D., Alhassan, A. I., Lee, C., Ley, R., Nakamura, S. and DenBaars, S. P., "High efficiency of III-nitride micro-light-emitting diodes by sidewall passivation using atomic layer deposition," *Opt. Express, OE* **26**(16), 21324–21331 (2018).
- [18] Kim, K., Hua, M., Liu, D., Kim, J., Chen, K. J. and Ma, Z., "Efficiency enhancement of InGaN/GaN blue light-emitting diodes with top surface deposition of AlN/Al<sub>2</sub>O<sub>3</sub>," *Nano Energy* **43**, 259–269 (2018).
- [19] Shockley, W. and Read, W. T., "Statistics of the Recombinations of Holes and Electrons," *Phys. Rev.* **87**(5), 835–842 (1952).
- [20] Yoshitsugu, K., Horita, M., Ishikawa, Y. and Uraoka, Y., "Characterizations of Al<sub>2</sub>O<sub>3</sub> gate dielectric deposited on n-GaN by plasma-assisted atomic layer deposition," *physica status solidi c* **10**(11), 1426–1429 (2013).
- [21] Long, R. D. and McIntyre, P. C., "Surface Preparation and Deposited Gate Oxides for Gallium Nitride Based Metal Oxide Semiconductor Devices," *Materials* **5**(7), 1297–1335 (2012).
- [22] Duan, T. L., Pan, J. S. and Ang, D. S., "Interfacial chemistry and valence band offset between GaN and Al<sub>2</sub>O<sub>3</sub> studied by X-ray photoelectron spectroscopy," *Appl. Phys. Lett.* **102**(20), 201604 (2013).
- [23] Martinez, G. L., Curiel, M. R., Skromme, B. J. and Molnar, R. J., "Surface recombination and sulfide passivation of GaN," *Journal of Elec Materi* **29**(3), 325–331 (2000).
- [24] Pearton, S. J., Yang, J., Cary, P. H., Ren, F., Kim, J., Tadjer, M. J. and Mastro, M. A., "A review of Ga<sub>2</sub>O<sub>3</sub> materials, processing, and devices," *Applied Physics Reviews* **5**(1), 011301 (2018).
- [25] Kroll, P., Dronskowski, R. and Martin, M., "Formation of spinel-type gallium oxynitrides: a density-functional study of binary and ternary phases in the system Ga–O–N," *Journal of Materials Chemistry* **15**(32), 3296–3302 (2005).
- [26] Kim, H., Kim, D. H. and Choi, B. J., "Interfacial and electrical properties of Al<sub>2</sub>O<sub>3</sub>/GaN metal–oxide–semiconductor junctions with ultrathin AlN layer," *Appl. Phys. A* **123**(12), 800 (2017).
- [27] Kang, H.-S., Reddy, M. S. P., Kim, D.-S., Kim, K.-W., Ha, J.-B., Lee, Y. S., Choi, H.-C. and Lee, J.-H., "Effect of oxygen species on the positive flat-band voltage shift in Al<sub>2</sub>O<sub>3</sub>/GaN metal–insulator–semiconductor capacitors with post-deposition annealing," *J. Phys. D: Appl. Phys.* **46**(15), 155101 (2013).
- [28] Mantler, M., Willis, J. P., Lachance, G. R., Vrebos, B. A. R., Mauser, K. E., Kawahara, N., Rousseau, R. M., Brouwer, P. N., Beckhoff, B., Kanngiesser, B., Langhoff, N., Wedell, R. and Wolff, H., "Quantitative analysis," [Handbook of Practical X-ray Fluorescence Analysis], Springer: Berlin, Germany, 309–410 (2006).

- [29] Martinez, E., Grampeix, H., Desplats, O., Herrera-Gomez, A., Ceballos-Sanchez, O., Guerrero, J., Yckache, K. and Martin, F., "Impact of vacuum anneal at low temperature on Al<sub>2</sub>O<sub>3</sub>/In-based III–V interfaces," *Chemical Physics Letters* **539–540**, 139–143 (2012).
- [30] Lin, Y.-J. and Lee, C.-T., "Surface analysis of (NH<sub>4</sub>)<sub>2</sub>Sx-treated InGaN using x-ray photoelectron spectroscopy," *Journal of Vacuum Science & Technology B: Microelectronics and Nanometer Structures Processing, Measurement, and Phenomena* **19**(5), 1734–1738 (2001).
- [31] Dingemans, G., Einsele, F., Beyer, W., van de Sanden, M. C. M. and Kessels, W. M. M., "Influence of annealing and Al<sub>2</sub>O<sub>3</sub> properties on the hydrogen-induced passivation of the Si/SiO<sub>2</sub> interface," *Journal of Applied Physics* **111**(9), 093713 (2012).